J Mater Sci (2019) 54:6971–6981

Composites

Magnetically sensitive nanocomposites based on the conductive shear-stiffening gel

Xiwen Fan[1], Sheng Wang[1], Shuaishuai Zhang[1], Yu Wang[1,*], and Xinglong Gong[1,*]

[1] CAS Key Laboratory of Mechanical Behavior and Design of Materials, Department of Modern Mechanics, CAS Center for Excellence in Complex System Mechanics, University of Science and Technology of China (USTC), Hefei 230027, People's Republic of China

Received: 16 November 2018
Accepted: 15 January 2019
Published online: 22 January 2019

ABSTRACT

In this paper a novel multi-functional composite with high electrical conductivity and excellent magnetic field sensitivity was fabricated by embedding carbon nanotubes (CNTs) and carbonyl iron powders (CIPs) into shear-stiffening gel (STG). Oscillatory shear test demonstrated its excellent rheological properties. When the mass fractions of CNTs and CIPs were 1 wt% and 50 wt%, the increase in storage modulus (G') reached 585% under 100 Hz oscillatory shear and 428% under 1.2 T magnetic flux density with respect to its initial state. The resistivity of this CNT–CIP–STG composite achieved 25 Ω m and showed strong dependence on the magnetic field. When the external magnetic flux density was 873 mT, the normalized electrical resistance response reached up to − 40.5%. Linearly increasing and step magnetic field was employed to study the electrical and mechanical behaviors of this CNT–CIP–STG composite. The instantaneous response and time effect were discussed. Interestingly, oscillatory shear showed limited influence on the electrical conductivity but notable enhancement on the sensitivity to magnetic field. A mechanic–electric coupling mechanism was proposed to illustrate enhancement of shear thickening effect and sensibility to magnetic field.

Introduction

Shear-stiffening (ST) polymer materials are an intelligent visco-elastic polymer whose storage modulus (G') and stiffness show orders of magnitude increment when the external shear frequency is beyond a critical value. Due to their sensitive rate-dependent properties, the ST polymer materials have great potential in the application of damping, vibration and controlling as well as personal body armor [1–6].

Lots of research works have been done on the shear-stiffening characteristic of the ST polymers [7–9]. Cross studied the rate-dependent properties of silicon-based polymer, silly putty, which was a typical shear-stiffening gel material [10]. They found that the compression speed had a serious impact on the

Address correspondence to E-mail: wyu@ustc.edu.cn; gongxl@ustc.edu.cn

https://doi.org/10.1007/s10853-019-03360-8

stiffness and the deformation behaviors. A standard visco-elastic model was developed for characterizing the viscous elastic properties of silly putty. Tian synthesized a novel shear-stiffening elastomer (STE) by silicone rubber and silicone oil [11]. The solid-to-liquid transition and the liquid-to-solid transition were observed in the STE sample when the shear rate was above a critical value in dynamic frequency sweep tests. Goertz studied the influence of temperature on the rheological property and concluded that the mechanical properties shifted significantly with respect to temperature [12]. Moreover, Palmer developed a new type of soft body armor based on polyurethane and ST polymers [13]. It was shown that the armor could absorb a large proportion of energy upon impact.

Recently, multi-functional smart materials have been attracting increasing interest because of their alternative chemical/physical/mechanical properties in different working environments [14–19]. For example, Borin showed that the composite based on a silicon polymeric matrix with embedded magnetic particles coated with a polymeric dielectric shell was highly sensitive to both magnetic and electric fields [20]. Yao prepared silver nanowire-based wearable multi-functional sensors, which could detect strain, pressure and finger touch with a fast response time and high sensitivity [21]. Due to the unique shear-stiffening characteristics and plastic behavior, the ST polymer would also be a good candidate material for multi-functional polymer composites. Wang fabricated a novel rate-dependent and self-healing conductive composite by dispersing multi-walled carbon nanotubes (CNTs) into a ST polymer matrix [22]. They found that the electrical conductivity changed accordingly when external stimulus was loaded, which meant that the composite could be used as a force sensor for body armors. Golinelli and Wang also found that, with the magnetic particle additives, the shear-stiffening gel would be endowed with special magnetically responsive characteristic [23, 24]. The shear-stiffening effect of magnetic shear-stiffening gel would increase correspondingly with the external magnetic field applied, which is a typical magneto-rheological (MR) effect. Obviously, the additives play an important role in determining the mechanical and physical properties of the shear-stiffening polymer under different working environments.

In this paper, a novel multi-functional smart composite (MFC) with ST performance, electrical conduction and MR effect was developed by dispersing the CNTs and magnetic particles into shearing-stiffening gel. The rheological experiments were conveyed, and this hybrid polymer material exhibited both excellent magneto-rheological properties and shear-stiffening properties. The electrical conductivity was tested to measure the percolation threshold. Linearly increasing and step magnetic field were loaded to study the electrical and mechanical response. Furthermore, the influence of oscillatory shear to magnetic-dependent properties was investigated, leading to a proposed coupling mechanism.

Experimental section

Materials

Boric acid, dimethyl siloxane, benzoyl peroxide (BPO) were used to prepare the gel matrix, which were purchased from Sinopharm Chemical Reagent Co. Ltd, Shanghai, China. Sodium dodecyl benzene sulfonate (SDBS) (Sinopharm Chemical Reagent Co. Ltd, Shanghai, China) was used as surfactant. Acetone and alcohol were purchased from Sinopharm Chemical Reagent Co. Ltd, Shanghai, China. The multi-walled carbon nanotubes (CNTs) with 3–5 nm in diameter and 8–13 μm in length were provided by Conductive Materials of Luelida Co. Ltd, Xinxiang City, Henan Province, China. And the magnetic particles were carbonyl iron particles (CIP, type CN), produced by BASF Germany. All the reagents were analytically pure and were used without additional purification.

Firstly, boric acid was heated in oven at 160 °C for 2 h to prepare pyroboric acid. Then, pyroboric acid and dimethyl silicone oil were mixed by mass ratio of 2:15, while some alcohol was added to improve the dispersion of pyroboric acid. The mixture was then heated at 250 °C for 8 h to obtain shear-stiffening gel (STG) matrix.

CNTs and CIPs were embedded into STG matrix in two steps. Firstly, the CNTs were dispersed. CNTs and SDBS (5:1 in mass ratio) were stirred in 200 ml solvent composed of acetone and alcohol with equal volume fraction. After 2 h, STG and BPO were added into the mixture in a mass ratio of 25:1. One hour later, the suspensions were collected into beakers and

ultrasonicated for 2 days for a better dispersion of the CNTs and volatilization of solution. Secondly, CIPs were homogeneously dispersed into the slurry by mechanical agitation. A two-roll mill (Taihu Rubber Machinery Inc., China, model XK-160) was adopted to make the materials uniform. All these samples were vulcanized at 83 °C for 2 h. In this experiment, the mass fractions of CNTs were 0.5 wt%, 1 wt%, 2 wt%, 3 wt% and the mass fractions of CIPs were 0 wt%, 30 wt%, 40 wt%, 50 wt%, 60 wt%, respectively. The samples were defined as CNT-x–CIP-y. Here the x and y represented the mass ratio of CNTs and CIPs.

Testing system

The morphology of CNTs, CIPs and the MFC was investigated by SEM (JEOL, JSM-6700F). The mechanical properties of the specimens were tested by a rheometer (Physical MCR 301, Anton Paar Co.). And an external magnetic field system was mounted on the rheometer. A programmable power supply (ITECH Electronic Co. Ltd, China) was used to supply constant current power. The magnetic flux density would range from 0 to 1.2 T by varying the exciting current in the range of 0–5 A. The rise time of square wave current in coil was within 0.1 s, which was much shorter than the measurement time for every point (1 s). The electrical resistance was measured by a Modulab Material Test System (MTS, Solartron analytical, AMETEK Advanced Measurement Technology, Inc., UK). A joint test system combining the rheometer, external magnetic field system and MTS is shown in Fig. 1 to characterize mechanical, magnetic and electrical properties of the MFC samples.

Parallel-plate geometry of the rheometer was adopted. The diameter was 20 mm, and the gap was set at 1 mm. All tested samples were molded into flat disks and pre-structured under 902 mT magnetic flux density for 300 s. The oscillation strain in the rheometer was limited at 0.1%. All the measurements were operated at 25 °C. The resistance was measured under 2 V DC mode, and the contact resistance of the system was 1.7 Ω.

Results and discussion

Microstructure characterization

Due to the heavy entanglements in the pristine CNTs (Fig. 2a), the large bundles seriously limited the interface interaction between polymer matrix and the CNTs which could not effectively improve the mechanical and physical properties of the composite [25–28]. Therefore, the CNTs were firstly treated with the ethanol and acetone solution to get better dispersion. And then ultrasonication was adopted for further dispersion of the CNTs. No obvious agglomeration could be observed in the treated CNTs (Fig. 2b). A two-roll mill was used to introduce the CIPs into STG matrix. When there were no CNTs added into the STG matrix, it could be clearly observed that there were obvious CIPs aggregates appeared on the surface of MFC (Fig. 2c), while the CNTs showed more effective interaction with the polymer matrix and perfectly integrated with the polymer matrix (Fig. 2d). No cracks or CIP aggregates could be observed in the surface of the MFC.

Rheological properties

Figure 3a shows the rate-dependent storage modulus (G') of the composite samples only containing CNTs. The G' for all the samples increased with increasing excitation frequency, presenting a pronounced ST effect. When excited by shear strain with the frequency set at 0.1 Hz, the G'_{min} of composites with 0.5 wt% CNTs was 1.0 kPa. When the frequency increased to 100 Hz, the G'_{max} reached 134.9 kPa, indicating a typical shear-stiffening property. Moreover, the content of the CNTs exhibited a significant influence on the mechanical properties of the composite. For the composite with 3 wt% CNTs, the G'_{min} and G'_{max} were 83.0 kPa and 889.9 kPa, respectively, indicating that the CNTs significantly strengthened the polymer matrix. With the addition of CIPs, it could be found that the mechanical properties could be further improved. As presented in Fig. 3b, the initial G'_{min} at 0.1 Hz was 8.19 kPa for CNT-1–CIP-0 wt% sample, while with the increase in CIPs mass fractions from 30 to 60 wt%, the initial G'_{min} increased from 31.29 to 262.80 kPa, and the maximum G'_{max} (100 Hz) came up to 1.05 MPa from 0.24 MPa.

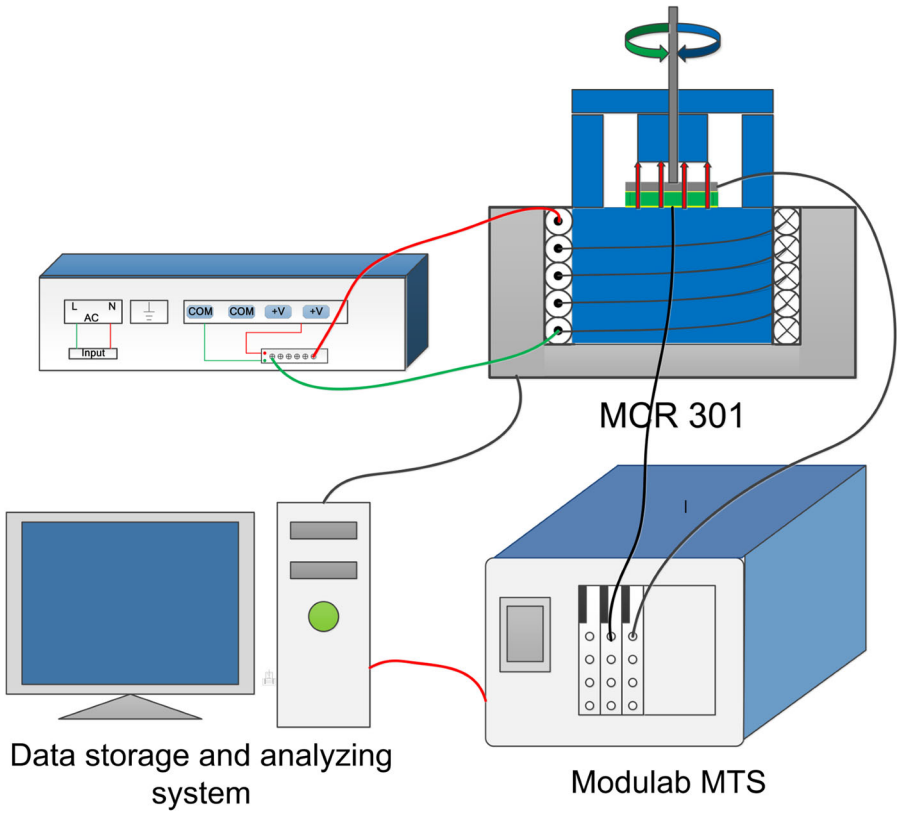

Figure 1 Schematic illustrations of the MTS and MCR 301 joint test system.

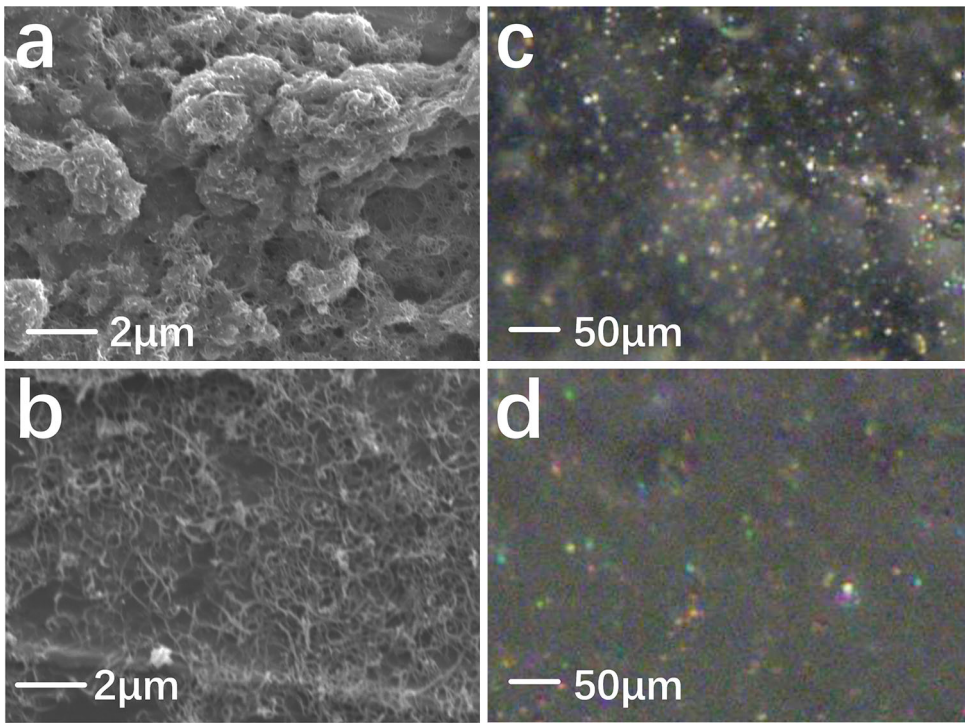

Figure 2 SEM images of primitive CNTs (**a**) and the dispersion-treated CNTs (**b**). The surface of STG only containing CIPs (CNT-0–CIP-50 wt%) (**c**) and MFC (CNT-1–CIP-50 wt%) (**d**) observed by optical microscope.

The magnetic-dependent behavior of the MFC was investigated under different external magnetic field strengths. Based on the above research, the mass fraction of CNTs was fixed at 1 wt%. The test frequency was 1 Hz, and strain amplitude was 0.1%. Note that the G' of samples with different contents of

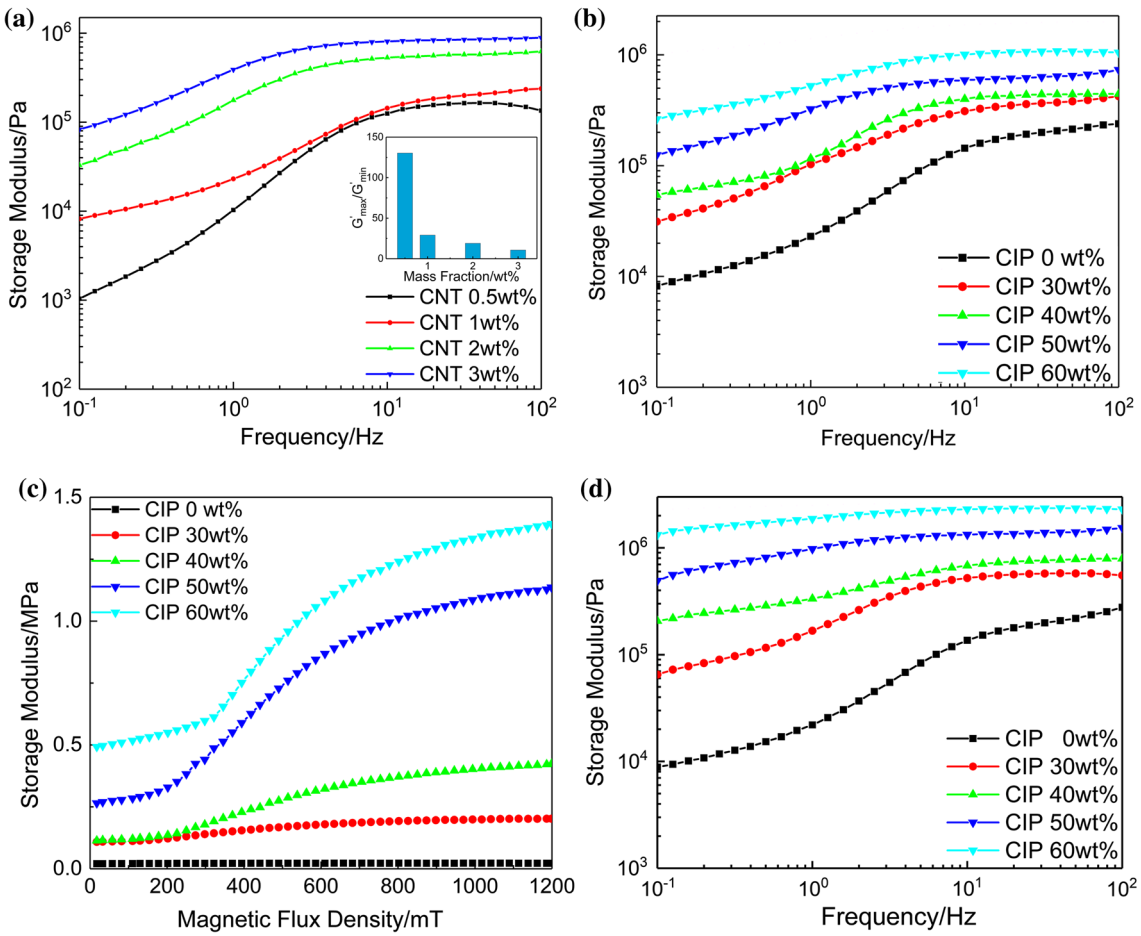

Figure 3 The rate-dependent characteristic (**a**) of different contents of CNTs and CIPs (**b**). The storage modulus versus magnetic flux density (**c**) with the 1 wt% CNTs. The rate-dependent character (**d**) at magnetic flux density of 873 mT.

CIPs exhibited remarkable MR effects (Fig. 3c). It was shown that there was an obvious tendency for the storage modulus to firstly increase with the increase in flux density of the external magnetic field and then reach a higher saturated plateau. In addition, the CIPs contents were observed to have great influence on G', which meant that higher CIPs contents induced a greater apparent MR effect. As for CNT-1–CIP-0 wt%, no magnetic field dependence occurred. As for other samples, a typical magnetic-dependent behavior was observed. The storage modulus of CNT-1–CIP-30 wt% increased from 0.109 MPa with the absence of magnetic field to 0.202 MPa at 1.2-T magnetic flux density. When the mass fraction of CIPs increased to 60 wt%, the storage modulus induced by magnetic field jumped to 1.393 MPa. It should be observed that the response of storage modulus to magnetic field could be divided into three stages: a slow growth region, a steep growth region and a saturation region. These three stages were obvious in the curve of CNT-1–CIP-60 wt%. The storage modulus of CNT-1–CIP-60 wt% increased from 0.492 to 0.612 MPa with the loading of 321 mT magnetic flux density. In the following magnetic field loading, from 321 to 634 mT, its storage modulus increased to 1.11 MPa. Then, the induced storage modulus stepped into a saturation region and increased to 1.39 MPa under 1.2 T magnetic flux density. With the increase in CIP contents, the critical point from the first stage to second stage moved backward and was more obvious. It was observed that the critical point of CNT-1–CIP-30 wt% and CNT-1–CIP-40 wt% was 178 mT. When the CIPs contents increased to 50 wt% and 60 wt%, the critical points moved to 202 mT and 322 mT. This transition should be owed to the competition of oscillation shear and magnetic field. Because of the presence of stable oscillation shear, the CIPs could not be

arranged in special direction with weak magnetic field. With the increase in magnetic field, the interaction between CIPs was intensified and exceeded the shear effect. Then, the first transition was observed. The second transition was caused by the saturated intensity of magnetization. Because of the drastic increase in the initial storage modulus, it showed that the ST effect had a tendency of weakening with the increase in mass fractions of additions. The storage modulus G' at 100 Hz was nearly four times as that at 0.1 Hz for CNT-1–CI-60 wt% sample, while the G'_{max}/G'_{min} was 29.1 for the CNT-1 wt%. With proper CIP content (CNT-1–CI-50 wt%), the MR effect achieved an increase in 428%, which was higher than previously reported MR elastomers. The composite still held its rate-dependent characteristic under magnetic field (Fig. 3d). For CNT-1–CIP-50 wt%, the minimum storage modulus at 0.1 Hz was 492.70 kPa and the max storage modulus at 100 Hz was 1.54 MPa, which were much higher than that without magnetic field. Based on the above experimental results, the mechanical properties of the polymer matrix could be effectively reinforced with the introduction of CNTs and CIPs. On the other hand, the ST effect still existed in the CNT–CIP–STG. More detailed data are shown in Tables 1 and 2. The coupling enhancement of stress and magnetic field adapted the composite to wider work environment.

The ST effect should owe to the behaviors of gel chain segments. As reported in other literature [26, 29], the transient "B–O cross-bonds" (Fig. 4a) in the polymer matrix played an important role in shear-stiffening characteristics. The "cross-bonds" were transient and mutable. They were much weaker than the covalent bonds. Therefore, under the stimulus in low rate, the B–O bond relaxed easily and it was easy for the gel chain segments to slip from each other. As a result, the composite had a lower storage modulus and behaved more like a fluid. However, at a higher shear frequency, the B–O bonds could not adapt to the external stimuli because of their longer relaxation time (Fig. 4b). Heavy agglomerations were generated inside the gel matrix. Thus, numerous cross-bonds would attract the entangled chains and impede the shift movement of these chains. Consequently, the MFC was more solidity. The excellent interaction between CNTs and gel chains increased the internal friction inside the composite, which made it more difficult for the slippage among the gel chain segments. Meanwhile, the free scope of the gel chains diminished for a large number of CNTs in the given volume [30, 31]. The MR effect is illustrated in Fig. 4c. The magneto-induced modulus (G') was mainly caused by the CIPs chains existed in the matrix whose interactions could be dramatically intensified by the external magnetic field. External magnetic field induced the microstructure to transform from isotropic to anisotropic. The CIPs concentrated in the direction of magnetic field and formed clusters, which provided resistance to shear deformation.

Table 1 Storage modulus (G') and loss modulus (G'') of CNT-1–CIP-y wt% under the oscillatory shear of 0.1 Hz and 100 Hz

Content (wt%)	CIP 0	CIP 30	CIP 40	CIP 50	CIP 60
G'_{min} (kPa)	8.19	31.29	54.46	124.60	262.80
G'_{max} (MPa)	0.23	0.42	0.44	0.73	1.05
G''_{min} (kPa)	6.68	20.71	26.44	69.26	108.40
G''_{max} (kPa)	18.97	19.81	21.54	25.38	50.24

Table 2 Storage modulus and loss modulus of CNT-1–CI-y wt% under the magnetic field

Content (wt%)	CIP 0	CIP 30	CIP 40	CIP 50	CIP 60
G'_0 (kPa)	20.35	109	110	260	490
G'_{max} (MPa)	0.02	0.24	0.42	1.14	1.39
G''_0 (kPa)	32.02	98.44	73.80	122.30	279.70
G''_{max} (kPa)	32.70	127.90	166.00	205.20	337.20

Percolation threshold and magnetic field-dependent electrical properties

The electrical performance of the MFC was studied by the Modulab Material Test System. Firstly, the samples containing only CNTs were tested to study the percolation threshold of CNTs in STG. It could be found that the electrical resistance changed from 4.1 to 2.8 kΩ, a sharp drop of over 1000 times with the CNT mass fraction from 0.5 to 1.0 wt% and the composite transformed from insulator to conductor. The percolation threshold was between 0.5 and 1.0 wt% as indicated in Fig. 5a. And the relationship between CIP contents and electrical resistance was invested (Fig. 5b). These samples all contained 1 wt%-CNT. With the mass fraction of CIPs

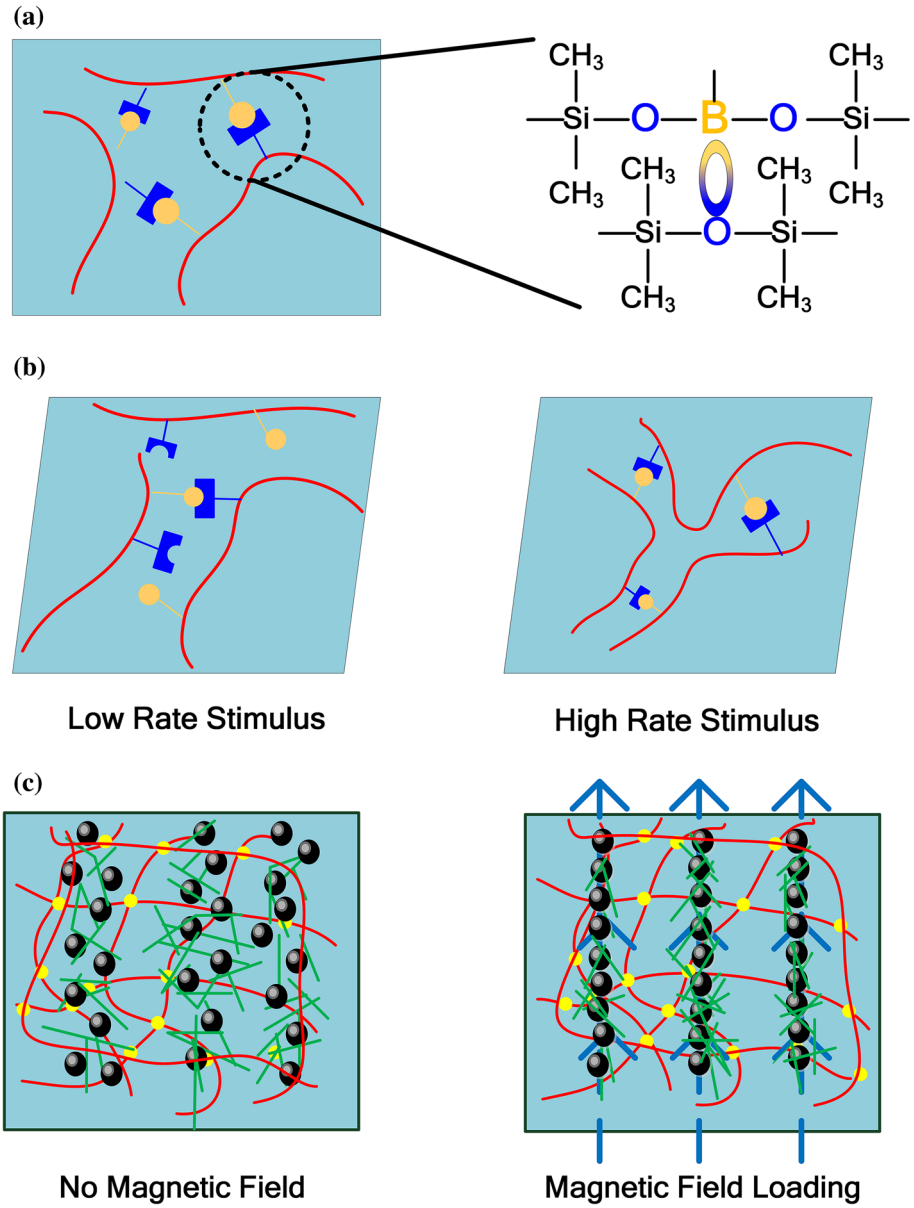

Figure 4 Illustration of rate-dependent and magnetic-dependent characteristic.

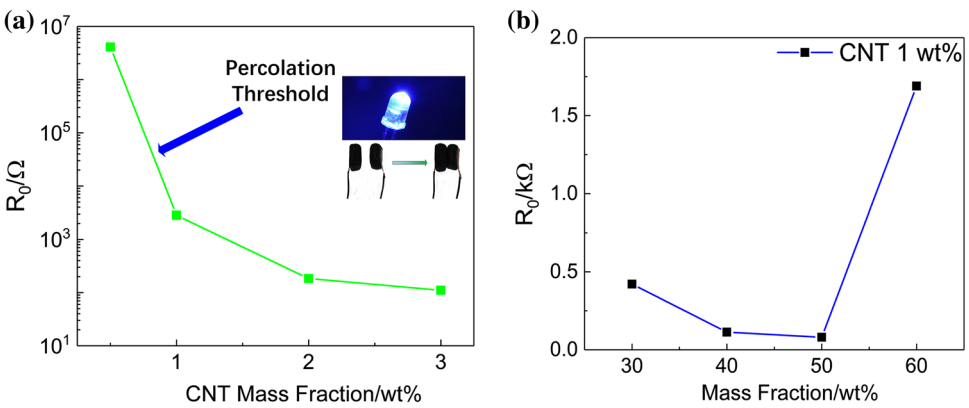

Figure 5 The electrical resistance versus the mass fraction of CNTs for the sample only contained CNTs (**a**) and for the sample CNT-1–CIP-*y* wt%, where *y* was 30, 40, 50 and 60, respectively (**b**).

increasing, the resistance of the composite decreased firstly and then abruptly jumped to a higher level. The composite achieved 25 Ω m in electrical resistivity when the mass fraction of CNTs and CIPs was 1 wt% and 50 wt%.

The bulk resistance consisted of three parts, $R = R_{CNT} + R_{CIP} + R_b$; here R_{CNT}, R_{CIP} and R_b were defined as the resistance contribution of CNTs and CIPs, and the contact resistances between CNTs and CIPs, respectively. As above discussed, the carbon nanotube had been uniformly dispersed in the matrix. It had been reported that when the gaps between nanotubes were small enough, the tunneling effects occurred and could form the effective conductive paths (ECPs) in the matrix (the red lines in Fig. 6a). With the addition of CIPs, small amount of CIPs helped interconnect the isolated CNTs and formed branch circuits, which led to a slight descent in resistance (Fig. 6b). When the mass fraction of CIPs reached 60 wt%, since the conductivity of CIPs was much weaker than that of CNTs, the aggregation of CIPs seriously broke up the ECPs and increased the resistance between different CNTs branches (Fig. 6c). As a result, the electrical resistance would sharply increase.

The electrical resistances under different external magnetic fields were further investigated with CIP mass fraction varying (Fig. 7a). The external magnetic flux density increased from 0 T to 900 mT. The relative change of the resistance was defined as $\Delta R/R_0 = (R_t - R_0)/R_0$. Here R_t and R_0 were the real-time electrical resistance under magnetic field and initial value, respectively. The relative resistance changes under 900 mT magnetic flux densities were − 1.1%, − 11.2%, − 24.7%, − 36.8%, − 32.4% when the mass fraction of CIPs changed from 0 to 60 wt%. As for each curve, the relative resistance change reduced with the magnetic flux density increased. When external magnetic field was applied on the sample, the CIPs would be driven to form particle chains and rearranged in special direction, leading to the space between the particles reduced. As a result, the distance between adjacent carbon nanotubes decreased and more CIPs could connect the small CNT branches to form the ECPs. Therefore, under the external magnetic field, the electrical resistances declined with the magnetic flux density increasing. As for the sample with 60 wt% CIPs, the abnormal magnetic sensitivity behaviors would be caused by the excessive aggregation of the CIPs in the polymer matrix under external magnetic field.

The transient responses of MFC under step magnetic field were further investigated. The results showed that when the step magnetic field was applied, the resistance reduced rapidly at first and then gradually stabilized. The relative resistance changes under 873 mT magnetic flux densities were − 19.1%, − 26.1%, − 40.5%, − 32.4%, when the mass fraction of CIPs changed from 30 to 60 wt% (Fig. 7b). Except the 60 wt% sample, the relative resistance change increased more with the mass fraction increased. The resistance declined rapidly at first and then gradually stabilized. An thought that the motion of CIPs under external magnetic field could be divided into two processes, chaining and clustering [32]. The chaining progress would be finished in very short time, but the clustering progress would continue much longer. As Fig. 7b shows, it can be seen that at the initial time, the resistance declined rapidly in the chaining process. After that, the resistance started to descend gently in the clustering process. The relative resistance change for CNT-1–CIP-50 wt% sample under different external magnetic flux densities is plotted in Fig. 7c. When the magnetic field was loaded, small decrease in resistance was observed. Then, the remarkable decline was observed

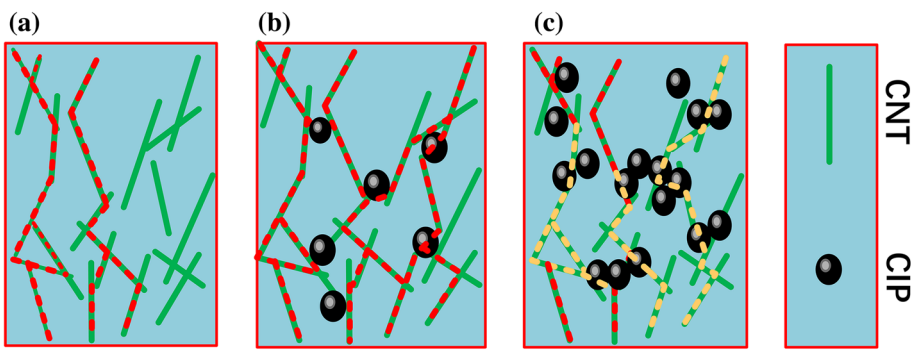

Figure 6 The effective conductive paths formed in the matrix (**a**). Small amount of CIPs would connect different CNTs branches (**b**). The aggregation of CIPs would break up the ECPs and increase the resistance between different CNTs branches (**c**).

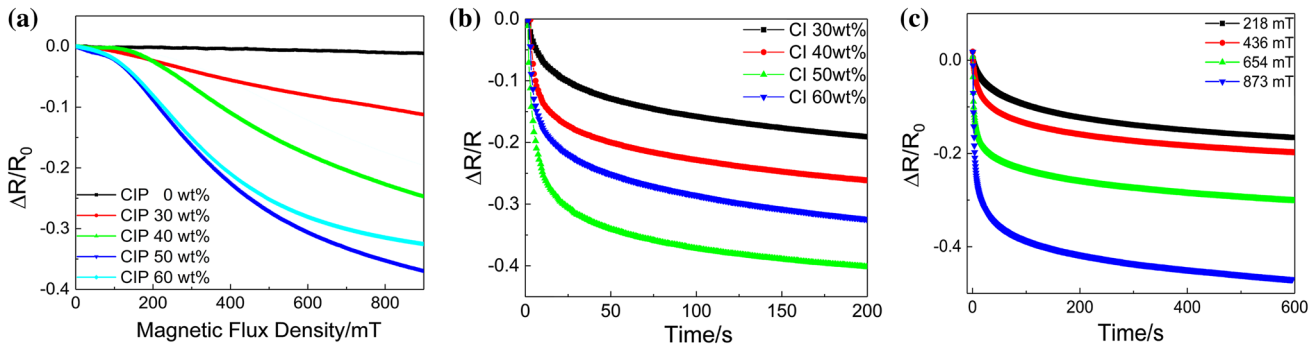

Figure 7 The resistance response to linearly increasing magnetic flux density (**a**) and step magnetic density (873 mT) (**b**) of CNT-1 wt%. The electrical resistance response to step magnetic flux density (**c**).

on the curves. After 600 s, the $\Delta R/R_0$ was − 16.55%, − 19.73%, − 30.17%, − 46.98% for magnetic flux densities of 218 mT, 436 mT, 654 mT, 873 mT, respectively. Higher magnetic flux density induced a more ordered arrangement of CIPs, which led to low resistances. Then, the cycle capacity was tested under 684 mT. A square wave magnetic field was used, with the field on for 15 s and then off for 10 s. In the short time of loading external magnetic field, the response of resistance mainly represented the chain progress of CIPs. With the extension of the loading time, the CIPs were more orderly than initial state. So a little decline could be observed in the peak value of electrical resistance.

Because the MFC showed typical rate-dependent characteristic, the electrical response to magnetic field under oscillatory shear was investigated. As shown in Fig. 3, the MFC showed typical elastic characteristics under high-speed shear compared to static state. Here 100 Hz oscillatory shear and 0.1% strain amplitude were adopted. Interestingly, the composite held its electrical properties constant under oscillatory shear (Fig. 8). In the sinusoidal oscillatory shear, the maximum displacement was 1 μm, which could hardly influence the arrangement and alignment of CNTs. Meanwhile, the overall volume had no change. So, the electrical characteristic kept constant.

Different magnetic flux densities were loaded on the composite with oscillatory shear, and the electrical resistance showed some differences from static state (Fig. 9a). Obviously, the response amplitude was larger than quasi-static state. Once the field is on, the electrical resistance rapidly declined. After maintaining the magnetic fields of 600 s, the values of $\Delta R/R_0$ were − 22.97%, − 54.38%, − 62.35% and − 71.13% which corresponded to magnetic field of

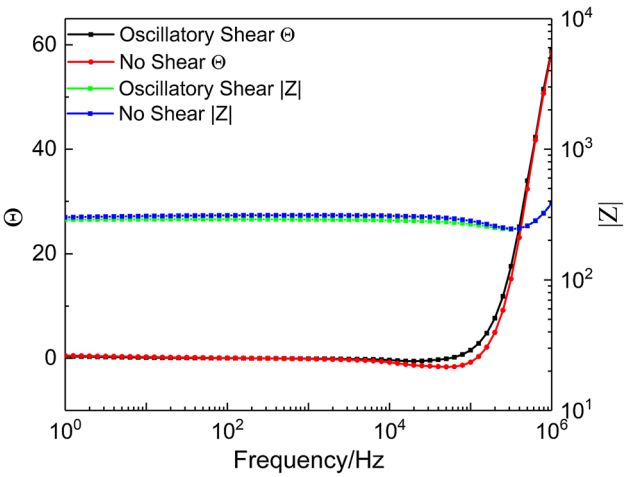

Figure 8 The Bode diagrams of the sample CNT-1–CIP-50 wt% with no shear and oscillatory shear deformation.

218 mT, 436 mT, 654 mT, 873 mT, respectively. Compared to no shear condition, the higher sensitivity to magnetic under oscillatory shear field should owe to the rate-dependent characteristic of gel matrix. The oscillation shear inverted the gel matrix from viscous to elastic. The elastic gel matrix could fasten the CNTs more tightly in the neighbor of CIPs and prevented slippage of the CNTs. Thus, the CNTs concentrated more in the direction of CIPs. Cycle stability of magnetic–electrical performance was compared between the oscillatory shear and no shear (Fig. 9b). Although the oscillatory shear had no effect on the electrical characteristic, it could significantly enhance the magnetic sensitivity of the MFC and the influence on the relative resistance change was stable.

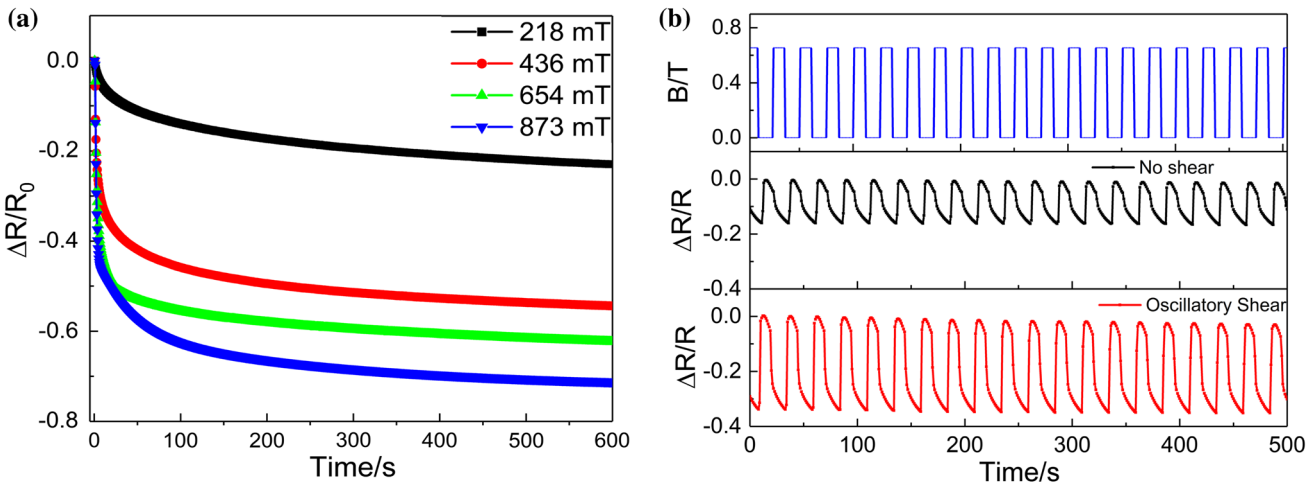

Figure 9 The electrical resistance responses to magnetic field under oscillatory shear (**a**) and its cycle stability of magnetic–electrical performance under square field (**b**).

Conclusion

In summary, we have developed a novel rate-dependent composite with high sensitivity to strain and magnetic field by dispersing CNTs and CIPs into STG polymer matrix. Different contents of CNTs and CIPs were explored to determine the appropriate ratio. According to the percolation theory and experimental results, the percolation threshold was between 0.50 and 1 wt%. The CNTs and CIPs both were favorable for the mechanical properties. The CNTs played a primary role in the electric property, and meanwhile, the CIPs could control the electrical properties by changing their aggregation state. CNT-1–CIP-50 wt% was the best proportion to balance the mechanical, electrical and sensitivity properties. This sample could achieve 585% increase in rate-dependent effect and 428% in magnet-dependent effect. The changes of electrical performance were synchronously tested. In addition, oscillatory shear could enhance the sensitivity to magnetic field. The composite showed potential application under dual excitation of shear force. A mechanism was proposed to illustrate the effect. Finally, the excellent mechanical and electrical property and good sensitivity to magnetic field made it a prospective material for future application in shielding and sensor area.

Acknowledgements

Financial supports from the National Natural Science Foundation of China (Grant No. 11572309), the Strategic Priority Research Program of the Chinese Academy of Sciences (Grant No. XDB22040502), the Fundamental Research Funds for the Central Universities (WK2480000002, WK2090050045) and China Postdoctoral Science Foundation (Grant No. 2018M632543) are gratefully acknowledged. This work is also supported by the Collaborative Innovation Center of Suzhou Nano Science and Technology.

References

[1] Xu CH, Wang Y, Wu J, Song S, Cao S, Xuan SH, Jiang WQ, Gong XL (2017) Anti-impact response of Kevlar sandwich structure with silly putty core. Compos Sci Technol 153:168–177

[2] He QY, Gong XL, Xuan SH, Jiang WQ, Chen Q (2015) Shear thickening of suspensions of porous silica nanoparticles. J Mater Sci 50(18):6041–6049. https://doi.org/10.1007/s10853-015-9151-5

[3] Hogg PJ (2006) Perspectives-composites in armor. Science 314(5802):1100–1101

[4] Liang J, Zhang XH (2015) Rheological properties of SP in shock transmission application. J Mater Civil Eng 27(9):04014250

[5] Lin XG, Guo F, Du CB, Yu GJ (2018) The mechanical properties of a novel STMR damper based on magnetorheological silly putty. Adv Mater Sci Eng 2018:2681461

[6] Wang Y, Ding L, Zhao C, Wang S, Xuan S, Jiang H, Gong X (2018) A novel magnetorheological shear-stiffening elastomer with self-healing ability. Compos Sci Technol 168:303–311

[7] Wagner HD, Lourie O, Zhou XF (1999) Macrofragmentation and microfragmentation phenomena in composite materials. Compos A 30(1):59–66

[8] Zhou W, Cui K, Tian N, Liu D, Liu Y, Meng L, Li X, He J, Li L, Li X, Tian F (2013) Disentanglement decelerating flow-induced nucleation. Polymer 54(2):942–947

[9] Chattaraj S, Pant P, Nanavati H (2018) Inter-relationships between mechanical properties of glassy polymers from nanoindentation and uniaxial compression. Polymer 144:128–141

[10] Cross R (2012) Elastic and viscous properties of silly putty. Am J Phys 80(10):870–875

[11] Tian TF, Li WH, Ding J, Alici G, Du H (2012) Study of shear-stiffened elastomers. Smart Mater Struct 21(12):125009

[12] Goertz MP, Zhu XY, Houston JE (2009) Temperature dependent relaxation of a "solid–liquid". J Polym Sci B Polym Phys 47(13):1285–1290

[13] Palmer RM, Green PC (2010) Energy absorbing material, U.S. Patent 7,794,827[P]

[14] Alam R, Lightcap IV, Karwacki CJ, Kamat PV (2014) Sense and shoot: simultaneous detection and degradation of low-level contaminants using graphene-based smart material assembly. ACS Nano 8(7):7272–7278

[15] Zambrzycki M, Fraczek-Szczypta A (2018) Conductive hybrid polymer composites based on recycled carbon fibres and carbon nanofillers. J Mater Sci 53(10):7403–7416. https://doi.org/10.1007/s10853-018-2062-5

[16] Lee JS, Shin KY, Cheong OJ, Kim JH, Jang J (2015) Highly sensitive and multifunctional tactile sensor using free-standing ZnO/PVDF thin film with graphene electrodes for pressure and temperature monitoring. Sci Rep 5:7887

[17] He S, Li H, Chen HL (2018) Preparation of light-sensitive polymer/graphene composite via molecular recognition by beta-cyclodextrin. J Mater Sci 53(20):14337–14349. https://doi.org/10.1007/s10853-018-2639-z

[18] Zhou G, Wang W, Peng M (2018) Functionalized aramid nanofibers prepared by polymerization induced self-assembly for simultaneously reinforcing and toughening of epoxy and carbon fiber/epoxy multiscale composite. Compos Sci Technol 168:312–319

[19] Boland CS, Khan U, Ryan G, Barwich S, Charifou R, Harvey A, Backes C, Li Z, Ferreira MS, Mobius ME, Young RJ, Coleman JN (2016) Sensitive electromechanical sensors using viscoelastic graphene–polymer nanocomposites. Science 354(6317):1257–1260

[20] Borin DY, Stepanov GV (2015) Elastomer with magneto- and electrorheological properties. J Intell Mater Syst Struct 26(14):1893–1898

[21] Ge J, Yao HB, Wang X, Ye YD, Wang JL, Wu ZY, Liu JW, Fan FJ, Gao HL, Zhang CL, Yu SH (2013) Stretchable conductors based on silver nanowires: improved performance through a binary network design. Angew Chem Int Ed 52(6):1654–1659

[22] Wang S, Xuan SH, Jiang WQ, Jiang WF, Yan L, Mao Y, Liu M, Gong XL (2015) Rate-dependent and self-healing conductive shear stiffening nanocomposite: a novel safe-guarding material with force sensitivity. J Mater Chem A 3(39):19790–19799

[23] Wang S, Jiang WQ, Jiang WF, Ye F, Mao Y, Xuan SH, Gong XL (2014) Multifunctional polymer composite with excellent shear stiffening performance and magnetorheological effect. J Mater Chem C 2(34):7133–7140

[24] Golinelli N, Spaggiari A, Dragoni E (2017) Mechanical behaviour of magnetic silly putty: viscoelastic and magnetorheological properties. J Intell Mater Syst Struct 28(8):953–960

[25] Kim GM, Yang BJ, Cho KJ, Kim EM, Lee HK (2017) Influences of CNT dispersion and pore characteristics on the electrical performance of cementitious composites. Compos Struct 164:32–42

[26] Liu Z, Pickeb SJ, Besseling NAM (2014) Polyborosiloxanes (PBSs), synthetic kinetics and characterization. Macromolecules 47:4531–4537

[27] Gkikas G, Barkoula NM, Paipetis AS (2012) Effect of dispersion conditions on the thermo-mechanical and toughness properties of multi walled carbon nanotubes-reinforced epoxy. Composites B 43(6):2697–2705

[28] Mittal G, Dhand V, Rhee KY, Park SJ, Lee WR (2015) A review on carbon nanotubes and graphene as fillers in reinforced polymer nanocomposites. J Ind Eng Chem 21:11–25

[29] Houston JE (2005) A local-probe analysis of the rheology of a "solid liquid". J Polym Sci Pol Phys 43(21):2993–2999

[30] Ma P-C, Siddiqui NA, Marom G, Kim J-K (2010) Dispersion and functionalization of carbon nanotubes for polymer-based nanocomposites: a review. Compos A 41(10):1345–1367

[31] Tkalya EE, Ghislandi M, de With G, Koning CE (2012) The use of surfactants for dispersing carbon nanotubes and graphene to make conductive nanocomposites. Curr Opin Colloid Interface Sci 17(4):225–231

[32] An HN, Sun B, Picken SJ, Mendes E (2012) Long time response of soft magnetorheological gels. J Phys Chem B 116(15):4702–4711